Dynamic simulation and optimization of a solar and waste heat assisted reverse brayton heat pump for industrial process heat upgrade

Panteleimon Tzouganakis[1,2*], Alberto Patti[3], Dimitrios Rakopoulos[1], Evangelos Bellos[2,1], Angelos Skembris[1], Nikolaos Rogkas[1] and Stefano Barberis[3]

[1] Centre for Research & Technology Hellas, Chemical Process & Energy Resource Institute, Athens, Greece

[2] Department of Mechanical Engineering, School of Engineering, University of West Attica, Athens, Greece

[3] Thermochemical Power Group, Department of Mechanical Engineering, University of Genoa, Genoa, Italy

*Corresponding Author: (p.tzouganakis@certh.gr)

Abstract:
Sustainable heat upgrade to high-temperature levels remains a critical challenge in industrial processes, due to their significant contribution to global CO_2 emissions. This work presents a novel concept that combines solar thermal energy and industrial waste heat to feed a high-temperature heat pump, which is based on the reverse Brayton cycle operating with air. Specifically, the proposed configuration couples solar thermal collectors with a storage tank using pressurized water as the storage medium. The stored thermal energy, together with waste heat, is employed as a source of a 150 kW_{th} reverse air Brayton heat pump capable of delivering the required high temperature demand. A dynamical MATLAB simulation model is developed to assess system performance under both summer and winter conditions. The examined case study considers a rubber industry located in Savona, Italy, where the useful process heat is provided at 250 ^oC with a diathermic oil of mass flow rate 10 kg/s. Furthermore, during the winter period, the system is designed to partially cover the facility's space heating demand. The system includes a solar thermal field of 300 m^2 collecting area and a thermal energy storage tank with a volume of 15 m^3, while the maximum available waste heat input is around 100 kW. The plant operates continuously, 24 hours per day and six days per week, throughout the year. Key performance indicators such as the mean daily coefficient of performance (COP), daily heat production, and the associated CO_2 emission reductions are calculated for both seasonal conditions. Finally, the influence of component sizing is investigated to maximize overall efficiency.

Keywords:
Heat upgrade, sustainable process heating, optimization, thermodynamic analysis, gross temperature lift

1. Introduction

The industrial sector is the third-largest source of carbon emissions in the European Union, generating approximately 720 megatons of CO_2 equivalent on a yearly basis. The total industrial energy consumption reaches close to 10 EJ, accounting for 26% of the global final energy demand, and approximately 4/5 of this energy is exploited for heat generation across a wide range of temperature levels [1]. Therefore, the high-temperature heat upgrading is essential for various industrial applications, including processes in the printing and food and beverage sectors [2], with nearly the 3/4 of this energy currently covered by fossil fuels [3]. In this direction, the development of technologies able to deliver the required thermal energy with low CO_2 emissions is of great importance for both industrial sustainability and environmental protection.

The integration of renewable energies into heat upgrading units can increase overall efficiency and make possible the achievement of high-temperature process heat [4]. Among these, solar thermal technologies have emerged as a promising option for sustainable industrial heating, especially in climates with high solar potential [5]. Also, waste heat streams of the industries can be effectively exploited by the heat upgrade machines and they can be hybridized with solar thermal systems. In parallel, heat pump technologies have gained attention as effective solutions for energy recovery and efficiency improvement because they operate by consuming green electricity, avoiding fossil fuel

consumption. Advances in this field include advanced thermodynamic cycle configurations, enhanced performance and reliability of system components [6]. Consequently, high-temperature heat pumps (HTHPs) are now capable of upgrading low-grade heat to temperatures exceeding 100 °C [3].

The performance of heat pumps strongly depends on the selection of a suitable working fluid. Various fluids have been investigated, with the optimal choice depending on factors such as operating temperature range, system capacity, critical characteristics of the fluids, environmental friendliness, safety issues and component design [6]. Common working fluids in HTHPs include hydrocarbons (e.g., propane, butane, etc.), fluorocarbons (e.g., R134a), and natural substances such as ammonia and CO_2 [3]. Over time, fluid selection has evolved, largely driven by environmental concerns and regulatory restrictions on substances with high environmental impact [7]. Zhang et al. [8] concluded that there is a need for continued research into new working fluids, particularly those suitable for high-temperature applications while maintaining low environmental impact. Moreover, safety issues, mainly regarding the flammability of many fluids, have to be considered. Moreover, the selection of the working medium depends on the temperature values of the available heat sources. As in power cycles, also in high-temperature heat pumps, different fluids and source temperatures lead to different optimal designs. Therefore, there are usual designs with vapor compression systems, absorption heat transfer, reverse Brayton high temperature heat pumps, and the research continues to evolve.

Despite extensive research on HTHPs, limited attention has been given to systems based on reverse Brayton cycles using air as the working fluid, with waste or solar energy as the heat source. Air offers notable advantages, including environmental neutrality and ease of handling. Furthermore, industrial compressors can achieve outlet temperatures exceeding 200 °C, with the potential to reach up to 400 °C. Therefore, the implementation of air-based Brayton cycle heat pumps for waste heat and solar energy utilization presents a promising opportunity for industrial applications.

This work aims to investigate the exploitation of solar energy to meet industrial energy demands by upgrading solar thermal output and recovering waste heat to produce high-temperature process heat. Also, the inclusion of a waste heat recovery unit that utilizes boiler flue gases is expected to enhance system efficiency. Patti et al. [9] proposed and analyzed a waste heat upgrade solution featuring the utilization of flue gases directly as the HTHP working fluid. Previous work by the authors [10] focused solely on solar-driven systems, while in the present study, both solar energy and waste heat recovery are considered together for enhancing the high-temperature heat pump performance. Additionally, the total system is designed to cover part of the plant's space heating demand, adding further novelty to this work. Specifically, the research involves the development of detailed numerical models for each system component to evaluate dynamic performance during the summer and winter periods. Key parameters examined include the solar field area, the ratio of solar field area to thermal storage volume, and the system's coefficient of performance (COP).

2. Materials and Methods

Figure 1 depicts the examined unit, which includes solar thermal (ST) collectors connected with a thermal energy storage (TES) tank that uses pressurized water at 16 bar as a storage medium. The water stored in the TES is further heated from a waste heat (WH) recovery unit that is installed to exploit the high-temperature flue gases from the boiler. The water then supplies heat to a 150-kW_{th} air-based reverse Brayton HTHP. After the HTHP source and before returning to the TES tank, the water is used in a space heating (SH) heat exchanger. The selected solar thermal collectors are evacuated flat plate collectors, which are a promising technology for industrial decarbonization. This concept belongs to the SOLINDARITY project, which investigates the efficient heat upgrade in various industries. One of the project's demonstration sites is the Artigo S.p.A., located in Savona, Italy. In this case study, a constant diathermic oil flow rate of 10 kg/s is needed to be upgraded from 245 ^{o}C to 250 ^{o}C on a 24/6 basis. The air-based reverse Brayton HTHP of Figure 1 shows three heat exchangers (HEX), a compressor, and a turbine. The goal of this unit is to augment the air temperature in HEX-3, which covers the industrial process heat, as well as to partially cover the space heating demand (secondary goal) in HEX-SH. The HTHP absorbs heat from hot water in HEX-1, while after this heat exchanger, the space heating demand is produced before the water returns to the TES tank. A recuperator (HEX-2) is used in the cycle to further heat up the air before entering the compressor. After the HEX-3, the air continues to the turbine to produce power and returns to HEX-1. The compressor and turbine are connected to the same shaft, which is electrically driven by a motor.

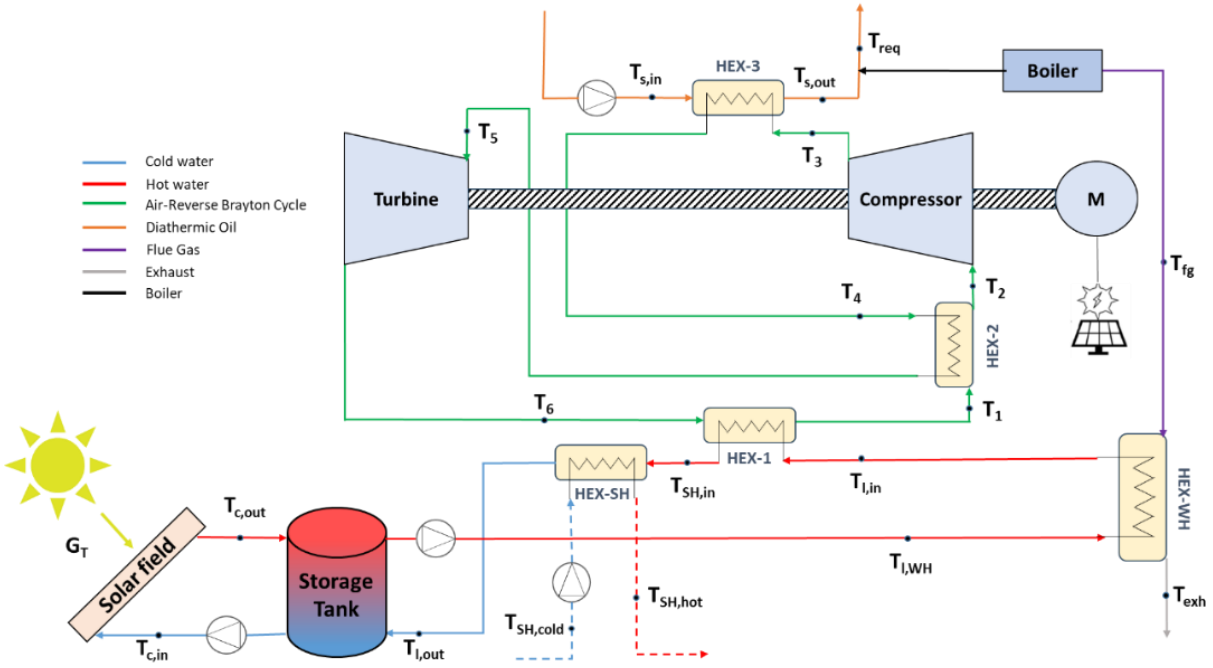

Figure 1. The studied systems include an HTHP, a solar thermal field, a thermal storage tank, a waste heat recovery unit and a space heating unit.

2.1. Solar Field

Solar energy is calculated by taking into account the weather data for the region of Savona, Italy, from PVGIS. Solar energy is given by Equation (1):

$$Q_{sol} = A_c \cdot G_T \tag{1}$$

where (Q_{sol}) is the solar energy, (A_c) is the total collecting area and (G_T) is the global solar irradiance. For the estimation of the global solar irradiation, parameters such as the direct normal and diffused irradiation (from weather data from the PVGIS database) and the longitude and latitude are taken into account. For the calculation of the useful heat, the efficiency of the solar collectors is considered [11]:

$$\frac{Q_u}{A_c} = n_{0,b} \cdot K_\theta(\theta) \cdot G_T - c_1 \cdot \left(T_{c,in} - T_{amb}\right) - c_2 \cdot \left(T_{c,in} - T_{amb}\right)^2 \tag{2}$$

where (T_{amb}) and ($T_{c,in}$) are the ambient temperature and water inlet temperature in the ST collectors, while (K_θ), ($n_{0,b}$), (c_1) and (c_2) are the incident angle modifier, and the thermal loss coefficients of the solar thermal collectors given by the manufacturer.

The useful heat (Q_u) is transferred to water circulating the ST collectors, is calculated as follows:

$$Q_u = \dot{m}_c \cdot C_{p,w} \cdot (T_{c,out} - T_{c,in}) \tag{3}$$

where ($\dot{m}_c$) is the total water mass flow rate of the ST collectors, ($C_{p,w}$) is the specific heat capacity, while ($T_{c,out}$) is the outlet temperature of the water from the ST field.

2.2. Thermal Energy Storage (TES) tank

The TES tank is commonly used in a system to store thermal energy. Its energy balance can be determined by considering the thermal input from the ST, the heat discharged from the tank, and the thermal losses to the environment. The tank is modeled using the mixing zone approach, as outlined in similar studies [12]. In this model, the TES tank is divided into N thermal zones, with each zone having a uniform temperature. The energy balance conditions at Zone-1, an intermediate zone (i.e., Zone-2), and Zone-N lead to the next relationships:

$$\frac{\rho_w V_t}{N} C_{p,w} \frac{\partial T_{st,1}}{\partial t} = \dot{m}_c C_{p,w}\left(T_{c,out} - T_{st,1}\right) + \dot{m}_l C_{p,w}\left(T_{st,2} - T_{st,1}\right) + \frac{U_t A_t}{N}\left(T_{amb} - T_{st,1}\right) \quad (4)$$

$$\frac{\rho_w V_t}{N} C_{p,w} \frac{\partial T_{st,2}}{\partial t} = \dot{m}_c C_{p,w}\left(T_{st,1} - T_{st,2}\right) + \dot{m}_l C_{p,w}\left(T_{st,3} - T_{st,2}\right) + \frac{U_t A_t}{N}\left(T_{amb} - T_{st,2}\right) \quad (5)$$

$$\frac{\rho_w V_t}{N} C_{p,w} \frac{\partial T_{st,N}}{\partial t} = \dot{m}_c C_{p,w}\left(T_{st,N-1} - T_{st,N}\right) + \dot{m}_l C_{p,w}\left(T_{l,out} - T_{st,N}\right) + \frac{U_t A_t}{N}\left(T_{amb} - T_{st,N}\right) \quad (6)$$

where (ρ_w) is the water density, (V_t) is volume, (U_t) is the thermal loss coefficient, (A_t) is the tank outer area, $(\dot{m}_l)$ is the mass flow rate from the tank to the HTHP, $(T_{l,out})$ is the water return temperature to the tank, while $(T_{st,i})$ is the temperature of the i^{th} thermal zone.

2.3. Waste Hear Recovery (WHR) unit

As depicted in Figure 1, the water after the tank is further heated by a WH recovery unit. The WHR unit exploits the high-temperature flue gases from the boiler to increase the temperature of the water before entering HEX-1. The modelling of the WH heat exchanger is derived by taking into account the energy equilibria as shown in Equations (11)-(13):

$$Q_{HEX-WH} = \dot{m}_l \cdot C_{p,w} \cdot (T_{l,in} - T_{l,wh}) \quad (7)$$

$$Q_{HEX-WH} = \dot{m}_{fg} \cdot C_{p,fg} \cdot (T_{fg} - T_{exh}) \quad (8)$$

$$Q_{HEX-WH} = UA_{HEX-WH} \cdot \Delta T_{lm,HEX-WH} \quad (9)$$

where $(\dot{m}_{fg})$ is the mass flow rate of the flue gases, $(C_{p,fg})$ is the specific heat capacity, (UA_{HEX-WH}) is the unit transfer area of the HEX-WH, $(T_{l,wh})$ is the water temperature from the tank before entering the WH recovery unit, $(T_{l,in})$ is the temperature of water entering HEX-1, (T_{fg}) and (T_{exh}) are the temperature of the flue gases (inlet of HEX-WH) and the exhaust (outlet of HEX-WH), respectively, and $(\Delta T_{lm,HEX-WH})$ is defined as follows:

$$\Delta T_{lm,HEX-WH} = \frac{\left(T_{fg} - T_{l,in}\right) - \left(T_{exh} - T_{l,,wh}\right)}{ln\left(\frac{T_{fg} - T_{l,in}}{T_{exh} - T_{l,,wh}}\right)} \quad (10)$$

Equations (7)-(10) can be solved by implementing the standard NTU method [13].

2.4. High Temperature Heat Pump (HTHP)

Finally, for the modelling of the HTHP, the energy equilibria and isentropic processes have been considered for HEXs and the compressor and turbine, respectively. The HEXs in the HTHP can be modelled following the same methodology as described for the HEX-WH. For instance, HEX-3 can be modelled from Equations (11)-(14):

$$Q_{HEX-3} = \dot{m}_s \cdot C_{p,s} \cdot (T_{s,out} - T_{s,in}) \quad (11)$$

$$Q_{HEX-3} = \dot{m}_a \cdot C_{p,a} \cdot (T_3 - T_4) \quad (12)$$

$$Q_{HEX-3} = UA_{HEX-3} \cdot \Delta T_{lm,HEX-3} \quad (13)$$

where $(\dot{m}_s)$ is the mass flow rate from the industrial process stream, $(C_{p,s})$ is the stream fluid specific heat capacity, $(\dot{m}_a)$ is the air mass flow rate, $(C_{p,a})$ is the air specific heat capacity, $(T_{s,in})$ and $(T_{s,out})$ are the inlet and outlet temperatures of the industrial stream, respectively, (T_3) and (T_4) are the air temperatures before and after HEX-3, (UA_{HEX-3}) is the unit transfer area of HEX-3 and $(\Delta T_{lm,HEX-3})$ is given as:

$$\Delta T_{lm,HEX-3} = \frac{\left(T_3 - T_{s,out}\right) - \left(T_4 - T_{s,in}\right)}{ln\left(\frac{T_3 - T_{s,out}}{T_4 - T_{s,in}}\right)} \quad (14)$$

A similar set of Equations is derived from HEX-1 and HEX-2. The compressor will increase the pressure of air in the cycle and, as a consequence, the temperature to meet the requirements in HEX-3. The power required in the compressor can be found from Equation (15):

$$P_{com} = \dot{m}_a \cdot (h_3 - h_2) \quad (15)$$

where (h_2) and (h_3) are the specific enthalpies before and after the compressor, and (P_{com}) the power required by the compressor. For the calculation of specific enthalpies, the isentropic efficiency of the compressor will be used, taking into account the compressor map provided by the manufacturer.
The power generated in the turbine is given by Equation (16):

$$P_{tur} = \dot{m}_a \cdot (h_5 - h_6) \tag{16}$$

where (h_5) and (h_6) are the enthalpies before and after the turbine and (P_{tur}) the power generated by the turbine. For the calculation of the specific enthalpies, the isentropic efficiency of the turbine will be used, taking into account the turbine map provided by the manufacturer.

The electric power of the motor can be calculated from Equation (17):

$$P_{el} = \frac{1}{n_{mot}} \left(\frac{P_{com}}{n_{m,com}} - n_{m,tur} \cdot P_{tur} \right) \tag{17}$$

where (n_{mot}) is the electric efficiency of the motor, ($n_{m,com}$) and ($n_{m,tur}$) are the mechanical efficiencies of the respective machines according to the subscripts, while (P_{el}) is the electric power.

From the equations' system of the HTHP, the air temperatures of the cycle and the required mass flow rates to achieve the desired temperature increase in HEX-3 can be calculated. It should be noted that the system of Equations is non-linear and therefore an iterative method is required for its solution.

Finally, the coefficient of performance (COP) can be determined from Equation (18):

$$COP = \frac{Q_{HEX-3}}{P_{el}} \tag{18}$$

2.5. Space Heating (SH) unit

The water from the outlet of HEX-1 will be used to provide space heating requirements, before returning to the TES tank, as shown in Figure 1. The modelling of the SH heat exchanger is obtained by considering the energy equilibria as shown in Equations (19)-(22):

$$Q_{HEX-SH} = \dot{m}_l \cdot C_{p,w} \cdot (T_{SH,in} - T_{l,out}) \tag{19}$$

$$Q_{HEX-SH} = \dot{m}_{SH} \cdot C_{p,w} \cdot (T_{SH,hot} - T_{SH,cold}) \tag{20}$$

$$Q_{HEX-SH} = UA_{HEX-SH} \cdot \Delta T_{lm,HEX-SH} \tag{21}$$

where ($\dot{m}_{SH}$) is the mass flow rate of space heating water, ($T_{SH,in}$) is the temperature at the HEX-SH inlet, consisting of the water coming from the HTHP source side outlet, ($T_{SH,cold}$) and ($T_{SH,hot}$) are the inlet and outlet temperatures on the space heating side, respectively, while (UA_{HEX-SH}) is the unit transfer area of HEX-SH and ($\Delta T_{lm,HEX-SH}$) is the log mean temperature difference of HEX-SH, which is defined as follows:

$$\Delta T_{lm,HEX-SH} = \frac{(T_{SH,in} - T_{SH,hot}) - (T_{l,out} - T_{SH,cold})}{ln\left(\frac{T_{SH,in} - T_{SH,hot}}{T_{l,out} - T_{SH,cold}}\right)} \tag{22}$$

The system of Equations (19)-(22) can be solved by implementing the standard NTU method.

2.6. System Control

To ensure a smooth and robust operation of the overall system, the following system control parameters will be implemented:

1. The ST-TES loop will operate if the global solar irradiance exceeds 150 W/m^2.
2. The TES-HTHP loop will stop its operation if the TES tank temperature drops below 90 ^{o}C.
3. The WHR and SH will operate only during winter.

2.7. Followed Methodology

To demonstrate the dynamical behavior of the suggested design, the following scenario was created to represent both summer and winter operation. Specifically, a representative summer week (6/8-12/8) and a representative winter week were chosen (21/1-27/1) to be examined in detail. Artigo, located in Savona, Italy, is the selected case study and it is operational from Monday morning at 09:00 to Saturday at 23:59. A MATLAB algorithm was developed to simulate the dynamical response of the system. At every time step of the simulation and in accordance with the system's control, the global solar irradiance and the useful heat from the solar collectors were found. The dynamic thermal behavior of the tank was calculated considering the mass flow rates and temperatures from the solar field and the return from the HTHP. In the tank, 20 thermal zones have been chosen after a suitable sensitivity investigation. Moreover, the time step of the analysis is chosen at 5 seconds to achieve a proper conversion of the results. Finally, the EBSILON® Professional tool was used for the simulation of the HTHP to facilitate the incorporation of the compressor/turbine maps, as well as pressure drops in the HEXs and in the piping, as is common in other scientific works (Jende et al., 2023). The HTHP system of Equations was solved for different inlet temperatures of water in HEX-1, to represent different operational conditions. The EBSILON® Professional tool calculated the required air mass flow rate and pressure ratio to meet the required output in HEX-3. As a result, a dynamical simulation was performed that included all components' interactions to obtain key insights into the system's performance. The parameters used in the selected case study are included in Table 1.

Table 1. Simulation parameters.

Parameters	Values
A_c	300 m^2
$\dot{m}_c$	6 kg/s
$\dot{m}_{fg}$	0.4 kg/s
$\dot{m}_l$	0.45 kg/s
$\dot{m}_s$	10 kg/s
$\dot{m}_{SH}$	2.5 kg/s
T_{fg}	250 °C
$T_{SH,cold}$	65 °C
$T_{s,in}$	245 °C
$T_{s,out}$	250 °C
U_T	0.5 $W/m^2/K$
V_t	15 m^3

3. Results & Discussion

3.1. Investigation of the main case study

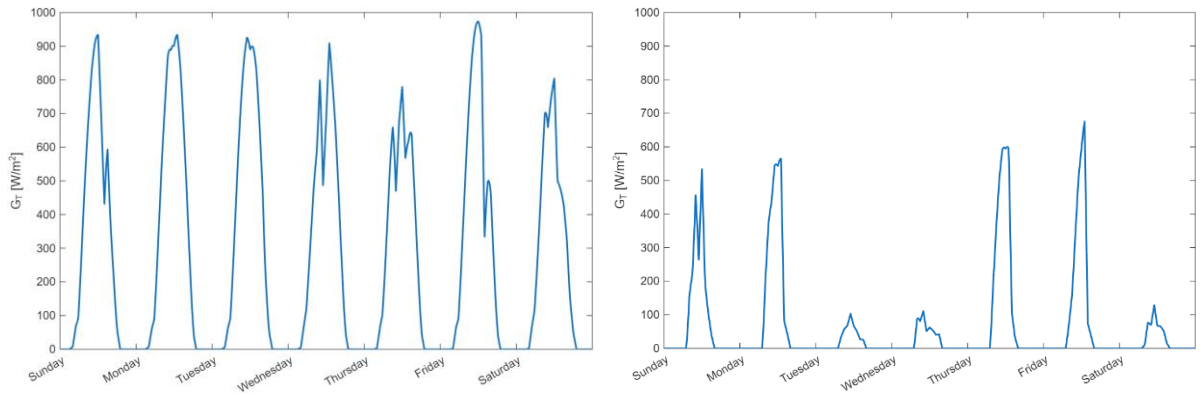

(a) Summer **(b) Winter**

Figure 2. Global solar irradiation during the studied weeks: (a) summer week, and (b) winter week.

Figure 2 depicts the expected global solar irradiation for Savona, Italy, as calculated from data obtained from PVGIS during the selected typical summer and winter weeks with respect to time. It is shown that the maximum global solar irradiation could reach 1000 W/m^2 during summer noon hours. However, during winter, the irradiation profiles appear to be fluctuating, which is attributed to bad weather conditions that are expected in Northern Italy.

Moreover, in Table 2, the HTHP results for different inlet temperatures of the water in the HEX-1 are presented with a constant sink inlet temperature of 245 °C, as obtained from the performed EBSILON® Professional simulations similar to the case investigated in [14]. It can be observed that the temperature of the water entering HEX-1 plays a critical role in improving the COP of the HTHP. The COP increases linearly with the inlet water temperature, with an increment of about 0.04 per 10 °C rise. This suggests that the optimal component (ST collectors and TES tank) sizing should ensure the highest possible inlet water temperature to HEX-1 throughout operation, in both summer and winter conditions.

Table 2. HTHP results for different inlet temperatures in HEX-1.

$T_{l,in}$ (°C)	$T_{SH,in}$ (°C)	Pressure ratio	m_a (kg/s)	P_{el} (kW)	COP
90	71.41	2.557	1.130	117.48	1.277
100	79.69	2.539	1.111	114.19	1.314
110	88.06	2.520	1.094	111.04	1.351
120	96.51	2.503	1.076	108.02	1.389
130	105.05	2.486	1.060	105.11	1.427
140	113.66	2.469	1.043	102.31	1.466
150	122.37	2.453	1.027	99.62	1.506
160	131.15	2.438	1.012	97.04	1.546
170	140.02	2.423	0.996	94.56	1.586

In Figure 3, the temperature of water at various points in the heat source cycle of the system is presented. During summer, the WHR and SH units are not operational, since the HTHP source demand can be fully covered by the ST field, while there are no space heating requirements in Artigo. The influence of the WHR unit during winter can be observed, as it increases the water temperature by approximately 40 °C, resulting in a significant increase in the COP of the HTHP. During summer noon hours, the temperature of the water entering HEX-1 is expected to reach approximately 160 °C, and as a consequence, the COP will have a value near the maximum.

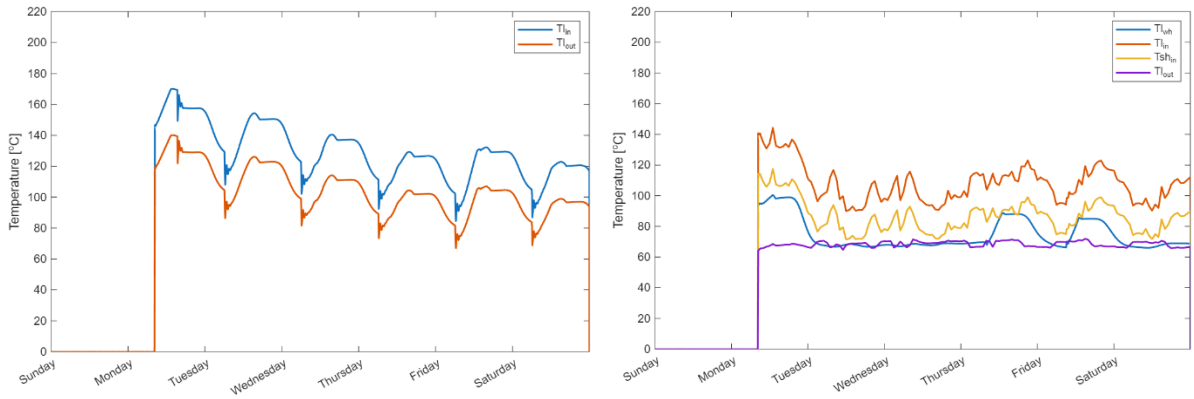

(a) Summer **(b) Winter**

Figure 3. Water temperature at various points of the TES-HTHP loop during the studied weeks: (a) summer week, and (b) winter week.

Figure 4 depicts the temperature of the water at different heights in the TES tank over time. The thermocline effect is evident during periods of high solar irradiation.

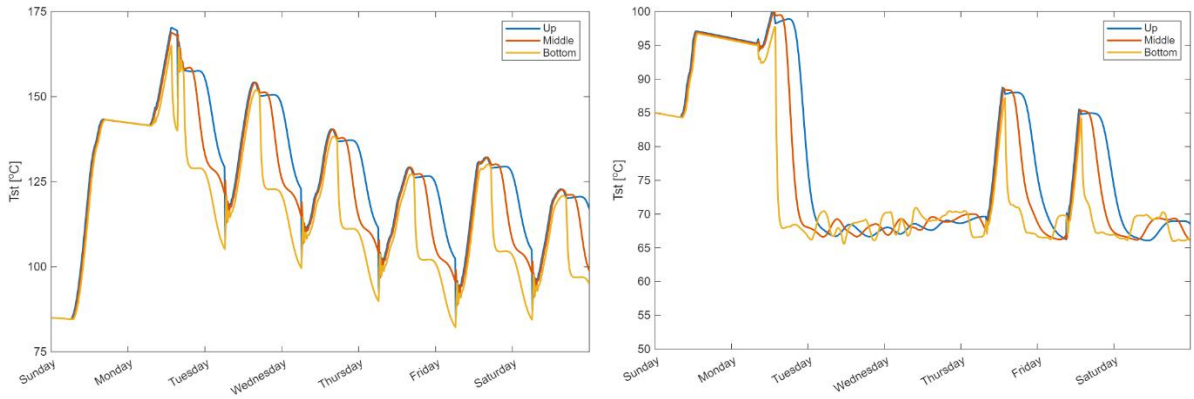

(a) Summer **(b) Winter**

Figure 4: TES temperature at different thermal zones during the studied weeks: (a) summer week, and (b) winter week.

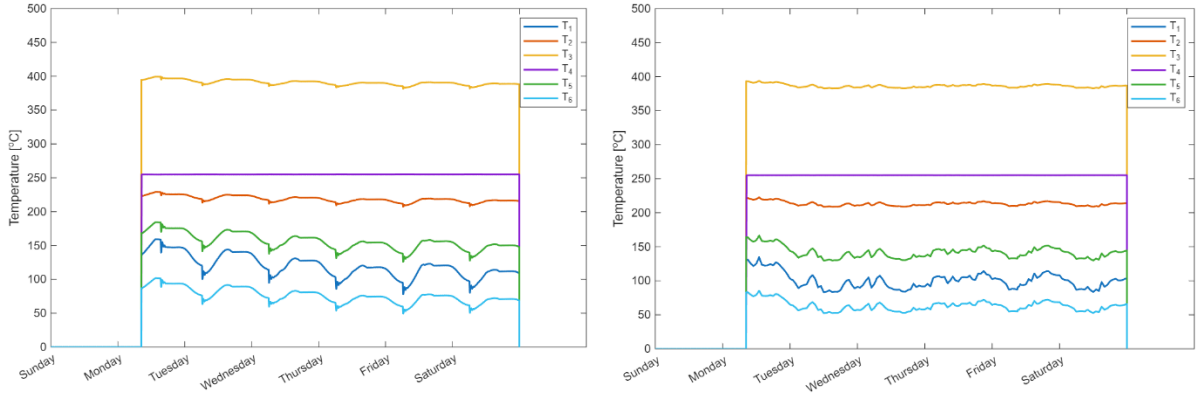

(a) Summer **(b) Winter**

Figure 5. Air temperatures in the HTHP during the studied (a) summer week and (b) winter week.

Figure 5 depicts the temperature at six different state points in the reverse air Brayton cycle, as shown in Figure 1. It can be observed that the HTHP exhibits similar behavior during both winter and summer, which is attributed to the WHR influence on the water's temperature in the inlet of HEX-1. Moreover, the electric power demand for driving the compressor–turbine shaft is presented in Figure 6. During noon hours in summer, the required electric power is reduced, as the water temperature in the TES tank is higher, as shown in Figure 4.

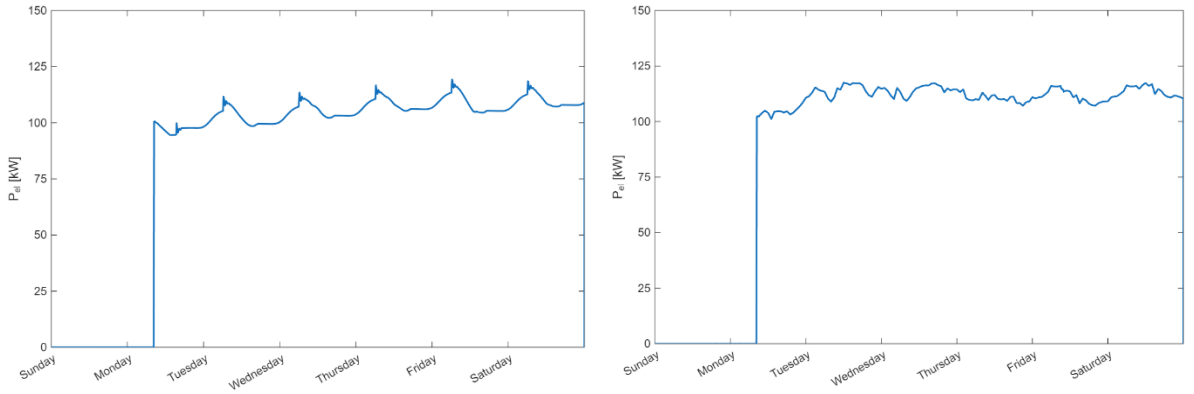

(a) Summer **(b) Winter**

Figure 6. Required electric power in the HTHP during the studied weeks: (a) summer week, and (b) winter week.

From the dynamical simulation of the system, the electric power demand for the operation of the HTHP is obtained, and then the COP calculation follows. Figure 7 presents the COP of the HTHP over time. It can be observed that the COP fluctuates between 1.30 and 1.55 during summer, and between 1.25 and 1.50 during winter. On Mondays, the COP of the HTHP is higher, as the TES is charged due to the fact that Artigo is closed on Sundays, as shown in Figure 4. In addition, during winter, the COP of the HTHP is significantly enhanced by the WHR, reaching values close to those observed in summer.

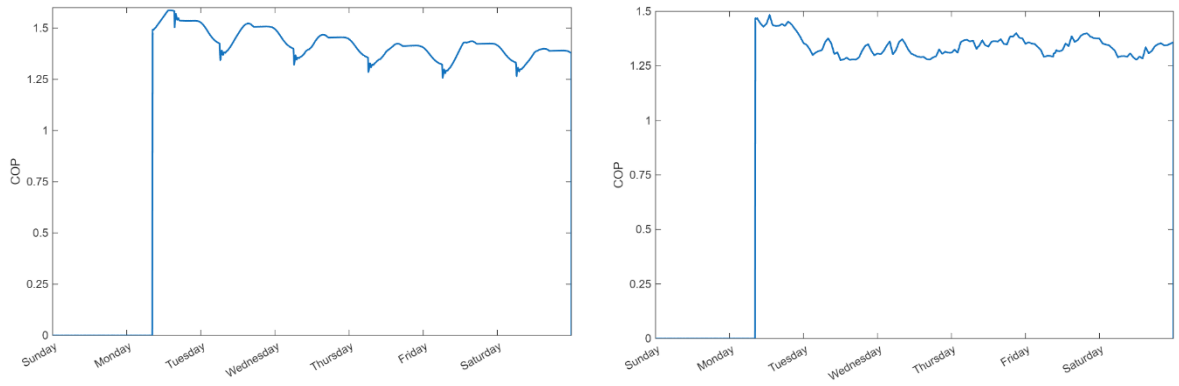

(a) Summer **(b) Winter**

Figure 7. COP variation during the studied weeks: (a) summer week, and (b) winter week.

Figure 8 shows the daily average COP of the HTHP. An average COP of 1.421 is observed during summer, while a value of 1.342 is observed during winter. The COP is higher on Mondays, as the TES tank exhibits higher temperatures, as shown in Figure 4. During the remaining days of the week, in both summer and winter, the COP remains stable, with minor fluctuations attributed to variations in solar irradiation, as shown in Figure 2.

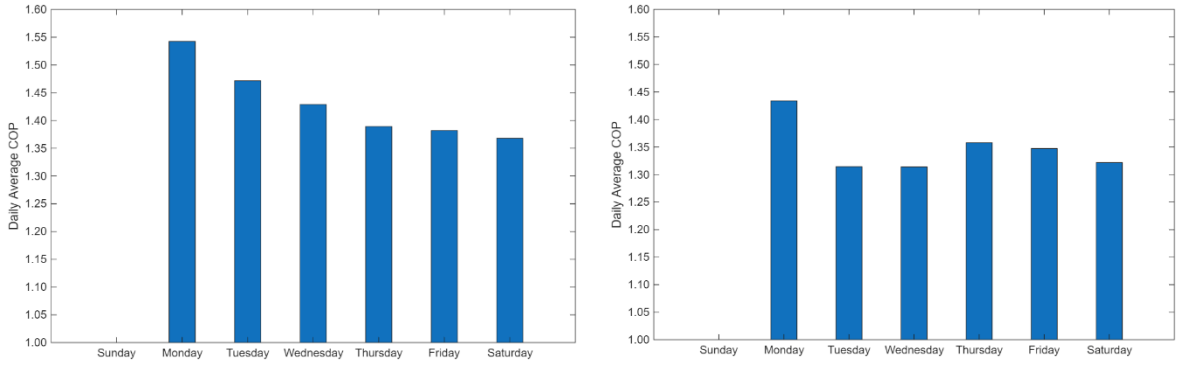

(a) Summer **(b) Winter**

Figure 8. Mean daily COP: (a) summer week, and (b) winter week.

Figure 9a presents the heat recovered from the WHR system during winter. The WHR provides an additional 50–90 kW, resulting in a significant increase in water temperature before entering HEX-1, as also shown in Figure 3. Figure 9b presents the SH power output. It can be observed that the system can provide up to 90 kW of heat on Mondays, which is attributed to the higher water temperature exiting HEX-1, as shown in Figure 3.

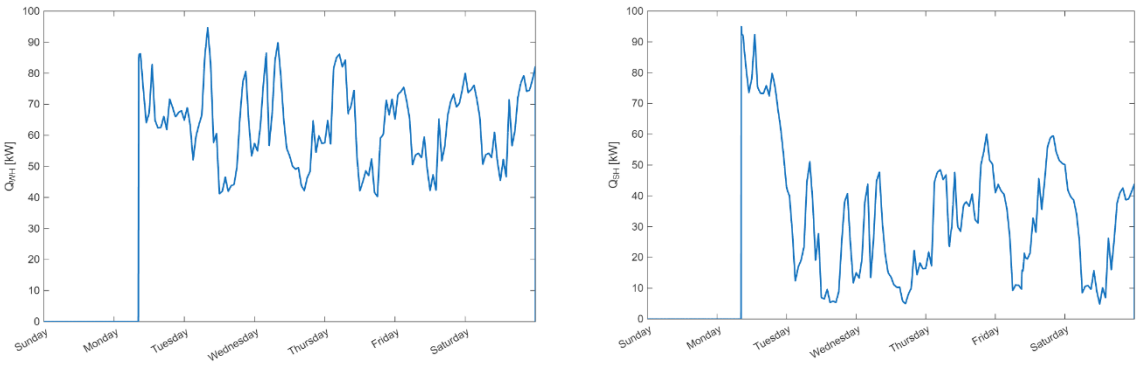

(a) **(b)**

Figure 9. WHR input (a) and SH output (b) during winter with respect to time.

3.2. Parametric investigation

A critical parameter that influences the performance of the HTHP is the temperature of the water entering HEX-1, as shown in Table 2. The TES tank temperature is directly related to both the total solar field area and the storage volume. Therefore, a parametric analysis of the impact of these two parameters on the COP of HTHP is necessary to achieve optimal performance. The analysis is conducted for both summer and winter conditions to determine the optimal configuration.

Figure 10 depicts the mean COP for various solar field areas and ratios of solar field area to storage volume. As expected, increasing the solar field area improves the COP of HTHP, particularly during summer when no WHR is available. During winter, the WHR assists in increasing the temperature of the water from the tank before it enters HEX-1, so the influence of the ST system is less significant. However, it should be noted that large solar collecting areas could lead to excess heat, since the HEX-1 requirements, combined with the absence of SH demand, result in a temperature buildup in the TES tank during summer. This may become problematic, as the ST system would need to incorporate a cooling mechanism to ensure that the water in the TES tank remains below saturation conditions. In addition, a ratio of 20 m²/m³ yields the highest average COP.

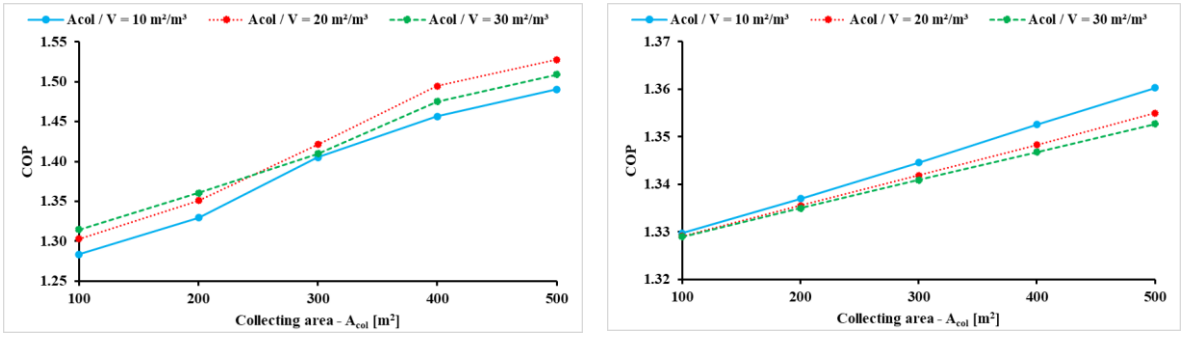

(a) Summer **(b) Winter**

Figure 10. Mean COP for various solar field areas and ratios of solar field area to the storage tank for: (a) summer week, and (b) winter week.

Therefore, based on the present parametric investigation, a configuration with a 300 m² collecting area and a 15 m³ TES tank (corresponding to a ratio of 20 m²/m³) is deemed to be the optimal selection for both summer and winter operation.

4. Conclusions

This work proposes a system for upgrading heat to high temperatures using solar energy and waste heat recovery. The system includes a solar thermal field, storage tank, waste heat recovery, a space heating unit, and a reverse Brayton heat pump. A MATLAB model simulates the system's operation at Artigo S.p.A. in Savona, Italy, where a temperature upgrade from 245 °C to 250 °C is required for a diathermic oil flow of 10 kg/s. The system consists of 300 m² of solar collectors, a 15 m³ TES tank, and a waste heat source corresponding to a flue gas mass flow of 0.4 kg/s at 250 °C. The performed simulations indicate a daily average COP of 1.412 in summer and 1.342 in winter. A parametric investigation of design parameters, including the solar field area and the ratio of solar field area to storage volume, was conducted to identify the optimal configuration for both summer and winter operation. Future research will extend the simulation to longer periods and integrate environmental and economic criteria for comprehensive system optimization. Additionally, the model could be improved by including heat losses in the piping, and a CFD analysis could be employed to verify the thermal response within the TES tank. Last but not least, the experimental investigation of such a system will make it possible to clearly validate the obtained results and also to extract very useful conclusions regarding the sustainability of reverse Brayton HTHPs in the real industrial environment.

Nomenclature

A	Area	[m^2]	**Subscripts**	
C_p	Specific heat capacity	[J/kg/K]	a	Air
COP	Coefficient of performance	[-]	amb	Ambient
G	Solar irradiation	[W/m^2]	c	Collector
h	Specific enthalpy	[J/kg]	com	Compressor
$\dot{m}$	Mass flow rate	[kg/s]	el	Electric
P	Power	[W]	fg	Flue gases
Q	Heat rate	[W]	in	Inlet
T	Temperature	[^oC]	l	TES- HTHP loop
U	Heat loss coefficient	[$W/m^2/K$]	out	Outlet
UA	Units of the transfer area	[W/K]	s	Heat sink
V	Volume	[m^3]	sol	Solar
Greek			t	tank
ρ	Density	[kg/m^3]	u	Useful
			w	Water

References

[1] Brodny, J., & Tutak, M. (2022). Analysis of the efficiency and structure of energy consumption in the industrial sector in the European Union countries between 1995 and 2019. *Science of the Total Environment*, *808*, 152052.

[2] Uusitalo, A., Turunen-Saaresti, T., Honkatukia, J., Tiainen, J., & Jaatinen-Värri, A. (2020). Numerical analysis of working fluids for large scale centrifugal compressor driven cascade heat pumps upgrading waste heat. *Applied Energy*, *269*, 115056.

[3] Badiei, A., Akhlaghi, Y. G., Zhao, X., Shittu, S., Xiao, X., Li, J., ... & Li, G. (2020). A chronological review of advances in solar assisted heat pump technology in 21st century. *Renewable and Sustainable Energy Reviews*, *132*, 110132.

[4] Sharevska, M., Sharevska, M., Brem, G., Hoogsteen, G., Hurink, J., & Hajimolana, Y. (2025). Systematic integration of high temperature heat pumps in industrial multi-energy systems. *Applied Thermal Engineering*, *278*, 127440.

[5] Farjana, S. H., Huda, N., Mahmud, M. P., & Saidur, R. (2018). Solar process heat in industrial systems–A global review. *Renewable and Sustainable Energy Reviews*, *82*, 2270-2286.

[6] Chua, K. J., Chou, S. K., & Yang, W. M. (2010). Advances in heat pump systems: A review. *Applied energy*, *87*(12), 3611-3624.

[7] Calm, J. M., & Hourahan, G. C. (2011, August). Physical, safety, and environmental data for current and alternative refrigerants. In *Proceedings of 23rd international congress of refrigeration (ICR2011), Prague, Czech Republic* (pp. 21-26).

[8] Zhang, J., Zhang, H. H., He, Y. L., & Tao, W. Q. (2016). A comprehensive review on advances and applications of industrial heat pumps based on the practices in China. *Applied Energy*, *178*, 800-825.
[9] Patti, A., Barberis, S., Traverso, A., Usai, V., & Spezia, R. (2026). Feasibility Study of a Brayton-Based High Temperature Heat Pump for Waste Heat Recovery in Industrial Applications. *Journal of Engineering for Gas Turbines and Power*, *148*(2), 021001.
[10] Tzouganakis, P., Bellos, E., Rakopoulos, D., Skembris, A., & Rogkas, N. (2025). Thermodynamic analysis of a solar-fed heat upgrade system using the reverse air brayton cycle. *Renewable Energy*, *238*, 121975.
[11] Fischer, S., Heidemann, W., Müller-Steinhagen, H., Perers, B., Bergquist, P., & Hellström, B. (2004). Collector test method under quasi-dynamic conditions according to the European Standard EN 12975-2. *Solar Energy*, *76*(1-3), 117-123.
[12] Bellos, E., & Tzivanidis, C. (2017). Parametric analysis and optimization of a solar driven trigeneration system based on ORC and absorption heat pump. *Journal of cleaner production*, *161*, 493-509.
[13] Lienhard, J. H. (2005). *A heat transfer textbook*. Phlogistron.
[14] Jende, E., Kabat, N., Stathopoulos, P., & Nicke, E. (2023). Thermodynamic analysis of an industrial process integration of a reversed Brayton high-temperature heat pump: A case study of an industrial food process. In *E3S Web of Conferences* (Vol. 414, p. 03006). EDP Sciences.

Acknowledgments

This work has been supported financially by the EU Horizon, research project SOLINDARITY (Grant agreement ID: 101136148).